Spin Electronics

Two-Dimensional Magnetic Semiconductors Based on Transition-Metal Dichalcogenides VX_2 (X = S, Se, Te) and Similar Layered Compounds VI_2 and $Co(OH)_2$

Huei-Ru Fuh[1], Kai-Wei Chang[2], Sheng-Hsiung Hung[3], and Horng-Tay Jeng[3, 4]

[1]Graduate Institute of Applied Physics, National Taiwan University, Taipei 106, Taiwan
[2]Research Center for Applied Sciences, Academia Sinica, Taipei 11529, Taiwan
[3]Department of Physics, National Tsing Hua University, Hsinchu 30013, Taiwan
[4]Institute of Physics, Academia Sinica, Taipei 11529, Taiwan

Received 19 Aug 2016, revised 13 Oct 2016, accepted 18 Oct 2016, published 26 Oct 2016, current version 31 Jan 2017.

Abstract—We present a new type of two-dimensional (2D) magnetic semiconductor based on transition-metal dichalcogenides MX_2 (M = V, Co; X = S, Se, Te, I, OH) via first-principles calculations. The obtained band gaps of monolayer (ML) VS_2, VSe_2, and VTe_2 in the H-phase given from the generalized gradient approximation (GGA) are respectively 0.05, 0.22, and 0.20 eV, all with integer magnetic moments of 1.0 μ_B, while ML VI_2 and $Co(OH)_2$ in the T-phase exhibit energy gaps of 0.96 and 0.08 eV, respectively, with integer magnetic moments of 3.0 μ_B. The GGA plus on-site Coulomb interaction U (GGA + U) scheme, which takes the electron-electron correlations in 3d orbitals into account, enhances the exchange splittings, and raises the energy gap of these MLs up to 0.4 to 3 eV. They agree very well with our calculated gaps based on the hybridized functional Heyd–Scuseria–Ernzerhof (HSE) of 0.6 to 3 eV. The wide range of energy gaps provides flexible applications in spintronics. All the calculations demonstrate 100% spin polarized bands around the Fermi level for these MLs. Combining the semiconducting energy gap and the fully spin polarized valence and conduction bands in a single-layer MX_2, this new type 2D magnetic semiconductor shows great potential in future spintronics applications.

Index Terms—Spin electronics, two-dimensional materials, magnetic semiconductor, transition-metal dichalcogenides.

I. INTRODUCTION

In recent years, semiconductor-based spintronics has attracted worldwide attention because of the possible spin current transport without the presence of a net charge current, which can avoid problems arising from capacitances and Joule heating [Montoya 2014]. For example, pure spin currents have been successfully created by spin pumping [Heinrich 2011] or the spin Seebeck effect [Uchida 2010, Jaworski 2010] using thermal gradients across a ferromagnetic (FM) layer. In most cases, it involves yttrium–iron–garnet (YIG) $Y_5Fe_3O_{12}$ as the magnetic insulator and Pt as the spin current detector [Miao 2014, Hahn 2013], in which the spin current is transformed into an detectable transverse voltage by the inverse spin Hall effect [Flipse 2014, Hoffmann 2013]. A new type of magnetoresistance in a Pt-YIG hybrid structure has been discovered [Miao 2014, Hahn 2013] and used in magnetic data transformation and memory storage [Chappert 2007, Fert 2008, Wolf 2001, Moodera 1988, Leclair 2002].

Next-generation spintronic devices can rely on room-temperature ferromagnetic semiconductors or heterostructures combining ferromagnetic metals with non-magnetic semiconductors. Nevertheless, searching for semiconducting magnetic materials with higher T_C and strong ferromagnetism is extremely difficult due to the conflicting requirements in the crystal and electronic structures of semiconductors and ferromagnets [Wolf 2001]. To date, almost all the discovered ferromagnetic semiconductors exhibit magnetic order well below room temperature, e.g., EuO ($T_C = 77$ K [Leclair 2002]), $BiMnO_3$ ($T_C = 100$ K [Kimura 2003]), La_2 $NiMnO_6$ ($T_C = 280$ K [Rogado 2005]), and diluted magnetic semiconductor (DMS) such as the prototypical system (Ga, Mn)As and the newly reported $(Ba_{1-x}K_x)(Zn_{1-y}Mn_y)_2As_2$ ($T_C = 185$ K, 180 K [Zhao 2013]). The only exception is the ferrimagnetic insulator YIG with a very high T_C of ~ 550 K [Hansen 1983] far beyond the room temperature. This is why most of the related works rely on YIG. Meanwhile, all of the known magnetic semiconductors are three-dimensional (3D) bulk materials.

Two-dimensional (2D) materials such as graphene, boron nitride, and the transition-metal dichalcogenides (TMDs) [Radisavljevic 2011, Ma 2011, Splendiani 2010, Meziane 2013, Kumar 2015] with single-layer thickness less than 1 nm have attracted tremendous attention in recent years. Because of the more than 40 different families [Marseglia 1983, Ataca 2012, Chhowalla 2013] and the rich electronic properties that can provide extensive applications, the TMD has become one of the most rapidly growing research fields. Representative TMDs such as MoS_2, $MoSe_2$, WS_2, and WSe_2 in the monolayer form are identified as direct-band-gap semiconductors. Giant spin splittings of 148–456 meV resulting from missing inversion symmetry and existing spin-orbit coupling (SOC) with the time-reversal symmetry preserved [Radisavljevic 2011, Zhu 2011, Kuc 2011] could be of high potential in spintronics. But it is still a challenge to coordinate the TMDs into nanoelectronics [Xiao 2012, Wang 2012]. Therefore, developing a new type of 2D TMD with exotic electronic properties is imperative.

Very recently, magnetism in TMD ultra-thin film has attracted increasing attention because of the successful synthesis of few-layer

Corresponding author: H.-T. Jeng (jeng@phys.nthu.edu.tw).
Digital Object Identifier 10.1109/LMAG.2016.2621720

vanadium disulfide (VS_2) [Feng 2008, Coleman 2011, Gao 2013]. The intrinsic ferromagnetism in these few-layer TMDs and their potential applications has drawn particular interest [Feng 2008, Zhang 2013, Ma 2012, Fu 2016]. The magnetic coupling strength and magnetic moments of these ultrathin nanosheets could be tuned by the isotropic strain [Ma 2012]. The intrinsic ferromagnetism provides a new opportunity for fabricating 2D ferromagnetic TMDs without introducing magnetic ions or tensile strains [Ma 2012]. The synthesis procedures are flexible for other VX_2 such as VSe_2 and VTe_2 monolayers. In addition to the bulk VX_2 [Chhowalla 2013], recent phonon dispersion studies reveal the stability of the monolayer VX_2 [Ataca 2012].

In this work, we systematically investigate the electronic structures of monolayer MX_2 (M = V, Co, X = S, Se, Te, I, OH) in the H- and T-phase based on the standard generalized gradient approximation (GGA), the GGA plus on-site Coulomb interaction (GGA + U) scheme taking into account the strong correlation effect in transition-metal ions, and the hybridized Heyd–Scuseria–Ernzerhof (HSE) functional accounting for the well-known underestimation of the semiconducting band gaps within the density function theory (DFT). We demonstrate that in all approaches these monolayers exhibit semiconducting energy gaps with intrinsic ferromagnetism, achieving an exceptional 2D magnetic semiconductor group.

II. COMPUTATIONAL DETAILS

The electronic structure calculations of monolayer MX_2 are performed using the projector augmented wave method with the Perdew–Burke–Ernzerhof (PBE) GGA [Perdew 1996] as implemented in the VASP package [Blöchl 1994, Kresse 1993]. The energy cutoff of 400 eV is used for the plane-wave basis expansion with the total energy convergence criteria of 1×10^{-5} eV per unit cell. Gamma-centered k-grids $16 \times 16 \times 1$ were sampled over the 2D Brillouin zone. Optimized monolayer structures were obtained with the residual force and stress less than 0.01 eV/Å and 1.0 kBar, respectively. The on-site Coulomb energy U = 2–8 eV for V and Co 3d electrons [Solovyev 1993] are taken into account for the electron-electron correlation effects of the localized V and Co 3d orbital in the GGA + U [Liechtenstein 1995] calculations. To go beyond the standard GGA approach, calculations based on the HSE [Heyd 2003, 2006] functional have also been performed for comparison with the GGA and GGA + U energy gaps.

III. RESULTS AND DISCUSSION

A. H-Phase Monolayer VX_2, X = S, Se, Te

The lattice structure of the VX_2 monolayer in the H-phase is depicted in Fig. 1. In the H-phase MX_2 TMD monolayer, the M ion is sandwiched by two X ions with an AbA stacking sequence in the unit cell as shown in Fig. 1. The spin-polarized band structures of the H-phase monolayer VX_2 with X = S, Se, and Te along the high symmetry lines are shown in Fig. 2. The upper and lower panels show GGA and GGA + U results, respectively. The GGA calculations show spin-polarized bands around the Fermi level (E_F) with indirect band gaps of 0.05–0.22 eV originated from the exchange splitting of the V-dz ^{2} bands, and integer magnetic moments of 1.0 μ_B/f.u. (formula unit) for all the three cases. These results lead to the desirable 2D

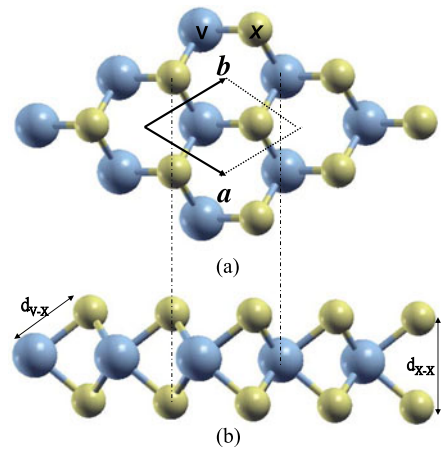

Fig. 1. The H-phase lattice structure of the monolayer VX_2 (X = S, Se, and Te). (a) and (b) are the top and side views, respectively. The blue and yellow spheres denote the V and X ions, respectively. $\boldsymbol{a}$ and $\boldsymbol{b}$ are the primitive lattice vectors of the 2D hexagonal unit cell.

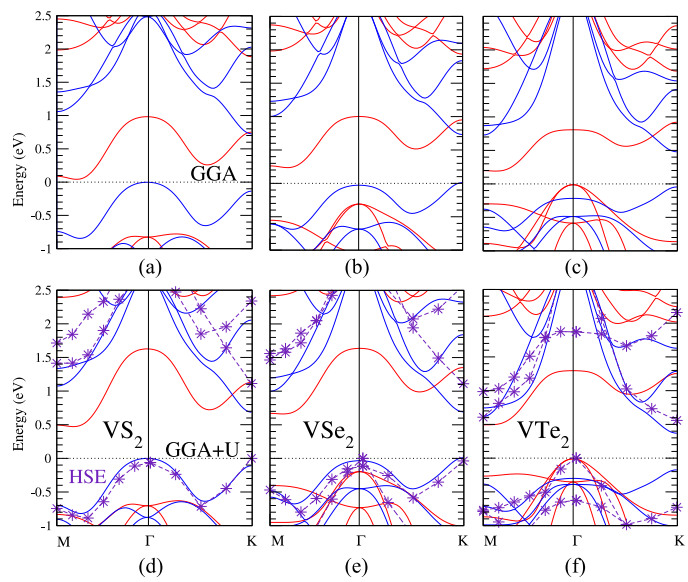

Fig. 2. Spin-polarized band structures of VX_2 monolayers without (upper panels) and with (lower panels) the on-site Coulomb energy (GGA + U) U = 2.0 eV and J = 0.87 eV for V 3d orbitals. The blue and red lines denote the spin up and down channels, respectively. The E_F (dotted horizontal line) is set at 0 eV. The HSE highest valence and lowest conduction bands are denoted by purple star symbols in the lower panels.

ferromagnetic semiconducting ground state. To examine the possible antiferromagnetism (AFM), we have adopted the $2 \times 2 \times 1$ supercell for the stripe type AFM arrangement. The calculated total energies demonstrate the ferromagnetic (FM) ground state for all the three VX_2 monolayers, being consistent with previous studies [Ma 2012, Abdul 2015, Houlong 2016]. Note that we have also performed calculations with the spin-orbit coupling (SOC) included self-consistently. The results of VS_2 and VSe_2 are more or less the same as those without SOC, while the VTe_2 part is slightly modified by SOC with the main character preserved.

To take into consideration the strong electron correlations in the relatively localized 3d orbitals, we perform GGA + U band structure calculations as shown in the lower panels of Fig. 2. The on-site

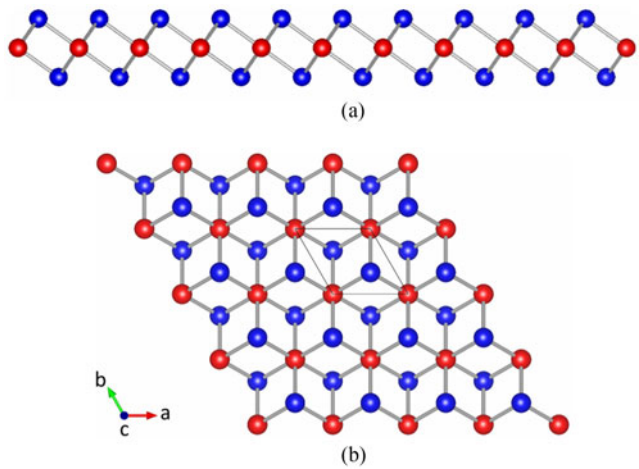

Fig. 3. The T-phase lattice structure of VI_2. (a) Side view, (b) top-view of the layered structure. Red and blue spheres denote the V and I ions, respectively. a, b, c are the lattice vectors. The black frame indicates the unit cell.

Coulomb repulsion U of 2 eV enhances the exchange splitting and gives rise to larger energy gaps of 0.473, 0.651, and 0.379 eV for VS_2, VSe_2, and VTe_2 respectively. Besides the significantly raised exchange gaps, the CBM and VBM locations of VS_2 and VSe_2 remain the same as those from GGA. But for VTe_2 the CBM from GGA + U locates at the K-point rather than around the M-point given by GGA. Finally, the combined SOC and on-site Coulomb repulsion U effect very slightly changes the GGA + U energy gaps. The broadest energy gap obtained from standard DFT (GGA and GGA + U) calculations is 0.684 eV of VSe_2, which is adequately large for real applications.

As mentioned above, the on-site Coulomb repulsion U of 2 eV used in this work is given from a previous theoretical estimation for V atoms [Liechtenstein 1995]. Since the U value of the same element in different materials also depends on the ionicity and the composition of the embedded compound, the precise value of U in VX2 is actually unknown. Because of the uncertainty of the U value, to go beyond the standard GGA and GGA + U approach, we also adopt the HSE hybridized functional to calculate the band structures of VX_2 monolayers as denoted by purple star symbols in the lower panels of Fig. 2 (only bands closest to Ef are depicted). The resultant HSE energy gaps are 1.110 eV, 1.150 eV, and 0.560 eV for VS_2, VSe_2, and VTe_2 monolayers, respectively. As can be seen, the most reliable HSE energy gaps around 1 eV are ideal for real applications

B. T-Phase Monolayer VI_2

The lattice structure of the VI_2 monolayer in the T-phase is depicted in Fig. 3. The T-phase VI_2 ML unit cell contains one V ion sandwiched by two I ions with an AbC stacking sequence as shown in Fig. 3. Experimentally the magnetism of bulk VI_2 is very complex. It shows frustrated AFM spin configuration in a very complicated manner. Below two Neel temperatures, it turns into ferromagnetic. It is the goal of this work to reveal if this bulk ferromagnetism in VI_2 remains in the monolayer phase.

The spin-polarized band structures of the T- monolayer VI_2 along the high symmetry lines from GGA, GGA + U with $U = 2$ eV, and HSE hybrid functional are shown in Fig. 4. All these calculations are

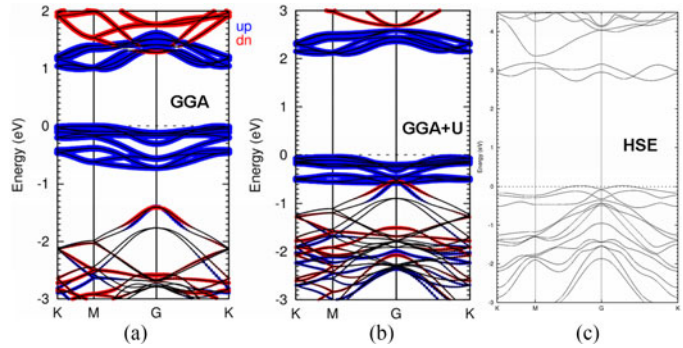

Fig. 4. Spin-polarized band structures of VI_2 monolayer from GGA (a), GGA + U with $U = 2$ eV for V-3d orbitals (b) and HSE (c). The spin-orbit coupling is included self-consistently in all these calculations because of the nontrivial SOC in I ions. The blue and red spheres denote the spin up and down components, respectively. The E_F (dotted horizontal line) is set at 0 eV.

done with SOC included self-consistently due to the nontrivial SOC in I ions. The GGA calculations [Fig. 4(a)] show spin polarized bands around the Fermi level (E_F) with an integer magnetic moments of 3.0 μ_B/f.u. The band gap of 0.96 eV originates from the exchange splitting of the V-dz ^{2} bands. Therefore, VI_2 ML also exhibits the desirable 2D ferromagnetic semiconducting ground state. We have also adopted the $2 \times 2 \times 1$ supercell for different type antiferromagnetism (AFM) arrangements to examine the possible AFM ground state. The calculated total energies demonstrate the ferromagnetic ground state for the VI_2 monolayer. Note that the spin-polarized valence and conduction bands all belong to the same spin channel due to the strong exchange splitting in the V-3d orbitals, which is presumably induced by the strong SOC in I ions. This is different from the case in the VS_2 series discussed previously.

To take the strong electron correlations in the relatively localized 3d orbitals into consideration, we perform GGA + U band structure calculations as shown in Fig. 4(b). The on-site Coulomb repulsion U of 2 eV enhances the exchange splitting and gives rise to larger energy gaps of 2.06 eV for VI_2 ML. Besides the significantly raised exchange gaps, the CBM and VBM locations remain the same as those from GGA. To see the trend of the U-effect, we have performed GGA + U calculations with U ranging from 2 to 5 eV for VI_2 ML. As expected, the energy gap is enhanced by the on-site U from ~ 1 eV ($U = 0$ eV) up to ~ 3 eV ($U = 5$ eV). To remove the uncertainty of the on-site U value, we also performed the hybridized functional HSE calculations as shown in Fig. 4(c). The energy gap given from HSE is 2.75 eV with the VBM and CBM positioned changed noticeably. The gap size also imply the on-site U value could be around 4 eV.

C. T-Phase Monolayer $Co(OH)_2$

Because of the recent great success of 2D materials such as graphene and transition-metal dichalcogenide monolayers, some layered metal hydroxides which crystallize in the hexagonal layered CdI_2-type crystal structures similar to the T-phase TMD have been fabricated by chemical methods. Although this family has been studied less, some have been found to be magnetic salts and therefore have attracted increasing attention. The lattice structure of the $Co(OH)_2$ monolayer in the T-phase is depicted in Fig. 5. The T-phase $Co(OH)_2$ ML unit cell

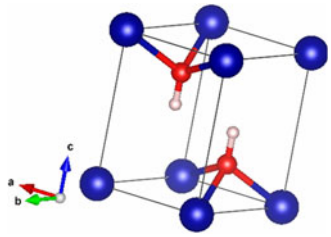

Fig. 5. The T-phase lattice structure of $Co(OH)_2$ ML. Blue, red, and white spheres denote the Co, O, and H ions, respectively. In this structure, the X ion is replaced by the OH hydroxide group ion with the oxygen ion bonded with the Co ion. a, b, c are the lattice vectors. The black frame indicates the unit cell.

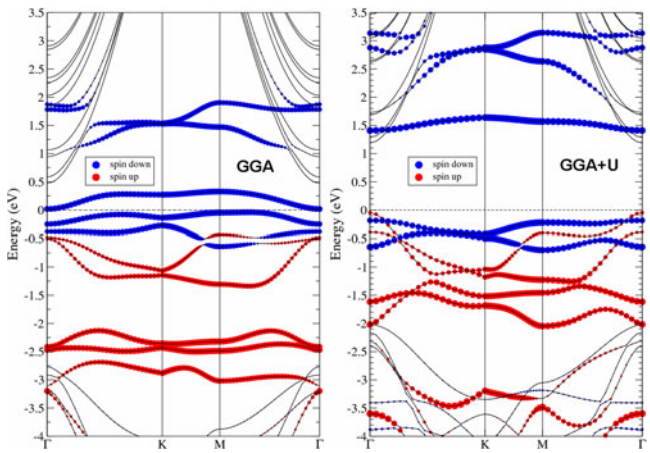

Fig. 6. Spin-polarized band structures of $Co(OH)_2$ monolayer from GGA and GGA + U with $U = 7.8$ eV for Co-3d orbitals. The spin-orbit coupling is included self-consistently in these calculations to take the magnetization direction into account. The red and blue spheres denote the spin up and down components, respectively. The E_F (dotted horizontal line) is set at 0 eV.

contains one Co ion sandwiched by two hydroxide (OH) ions with an AbC stacking sequence as shown in Fig. 5.

The spin-polarized band structures of the T-phase monolayer $Co(OH)_2$ along the high symmetry lines are shown in Fig. 6. The left- and right-hand-side panels show results from GGA and GGA + U with $U = 7.8$ eV, respectively. The SOC is included self-consistently in both calculations to take the magnetization direction into consideration. The GGA calculations show spin-polarized bands around the Fermi level with a small indirect band gap of 0.08 eV given from the exchange splitting of the Co-d bands. Following the Hund's rule for over half-filled 3d orbitals, the 5 spin-up Co-3d bands (red) are fully occupied while only 2 spin-down Co-3d bands (blue) are occupied, resulting in an integer magnetic moment of 3.0 μ_B/f.u. These characters demonstrate that $Co(OH)_2$ exhibits the desirable 2D ferromagnetic semiconducting ground state. To test the possible AFM ground state, we have adopted the $2 \times 2 \times 1$ supercell for various AFM arrangements. The calculated total energies demonstrate the ferromagnetic ground state for $Co(OH)_2$ monolayer with the magnetization direction (easy axis) along the crystal (110) direction.

Taking the strong electron-electron correlations in the relatively localized Co-3d orbitals into consideration, we perform GGA + U band structure calculations as shown in the right-hand-panel of Fig. 6. The on-site Coulomb repulsion U of 7.8 eV for the Co-3d orbital significantly enhances the exchange splitting and gives rise to larger energy gaps of 1.21 eV for ML $Co(OH)_2$. Besides the significantly raised exchange gaps, the CBM and VBM locations were different from those given by GGA because of the changed band dispersion. To see the trend of the U-effect, we also performed GGA + U calculations with U ranging from 1 to 8 eV for $Co(OH)_2$ ML. As expected, the energy gap was enhanced by the on-site U from ~0.1 eV ($U = 0$ eV) up to ~ 1.3 eV ($U = 8$ eV).

IV. CONCLUSION

We have presented theoretical investigations on a new type of 2D ferromagnetic semiconductor: MX_2 (M = V, Co, X = S, Se Te, I, OH) monolayer in H- and T-phase based on GGA, GGA + U, as well as HSE calculations. The standard GGA scheme gives exchange energy gaps of 0.046, 0.225, and 0.201 eV for VS_2, VSe_2, and VTe_2 H-monolayers, respectively, with integer magnetic moment of 1 μ_B/f.u. for all three cases. While ML VI_2 and $Co(OH)_2$ in the T-phase exhibit energy gaps of 0.96 and 0.08 eV, respectively, with integer magnetic moments of 3 μ_B. The 100% spin-polarized bands around E_F are mainly from the 3d local moments in the V and Co ions. The on-site Coulomb interaction $U = 2$–8 eV enhances the energy gaps to 0.4–3 eV. They agree well with the HSE energy gaps of 0.6–3 eV. Our study demonstrates the great potential of the MX_2 monolayers in spintronics and invites further experimental investigations on these ultrathin new types 2D ferromagnetic semiconductors.

ACKNOWLEDGMENT

H. R. Fuh thanks the computer and information networking center in National Taiwan University, Taiwan, for the computational support. H. T. Jeng acknowledges the support from NCTS, Ministry of Science and Technology, Academia Sinica, and National Tsing Hua University, Taiwan.

REFERENCES

Ataca C, Şahin H, and Ciraci S (2012), "Stable, single-layer MX_2 transition-metal oxides and dichalcogenides in a honeycomb-like structure," *J. Phys. Chem. C*, vol. 116, pp. 8983–8999, doi: 10.1021/jp212558p.

Abdul W A H M, Chakrabarty S, and Das G P (2015), "Quantum size effects in layered VX_2 (X = S, Se) materials: Manifestation of metal to semimetal or semiconductor transition," *J. Appl. Phys.*, vol. 117, 064313, doi: 10.1063/1.4908114.

Blöchl P E (1994), "Projector augmented-wave method," *Phys. Rev. B*, vol. 50, pp. 17953–17979, doi: 10.1103/PhysRevB.50.17953.

Chappert C, Fert A, and Van Dau F N (2007), "The emergence of spin electronics in data storage," *Nature Mater.*, vol. 6, pp. 813–823, doi: 10.1038/nmat2024.

Chhowalla M, Shin H S, Eda G, Li L-J, Loh K P, Zhang H (2013), "The chemistry of two-dimensional layered transition metal dichalcogenide nanosheets," *Nature Chem.*, vol. 5, pp. 263–275, doi: 10.1038/nchem.1589.

Coleman J N, Lotya M, O'Neill A, Bergin S D, King P J, Khan U, Young K, Gaucher A, De S, Smith R J, Shvets I V, Arora S K, Stanton G, Kim H-Y, Lee K, Kim G T, Duesberg G S, Hallam T, Boland J J, Wang J J, Donegan J F, Grunlan J C, Moriarty G, Shmeliov A, Nicholls R J, Perkins J M, Grieveson E M, Theuwissen K, McComb D W, Nellist P D, Nicolosi V (2011), "Two-dimensional nanosheets produced by liquid exfoliation of layered materials," *Science*, vol. 331, pp. 568–571, doi: 10.1126/science.1194975.

Feng J, Sun X, Wu C, Peng L, Lin C, Hu S, Yang J, Xie Y (2011), "Metallic few-layered (X = VS_2 ultrathin nanosheets: High two-dimensional conductivity for in-plane supercapacitors," *J. Am. Chem. Soc.*, vol. 133, pp. 17832–17838, doi: 10.1021/ja207176c.

Fert A (2008), "Nobel lecture: Origin, development, and future of spintronics," *Rev. Mod. Phys.*, vol. 80, pp. 1517–1530, doi: 10.1103/RevModPhys.80.1517.

Flipse J, Dejene F K, Wagenaar D, Bauer G E W, Ben Youssef J, van Wees B J (2014), "Observation of the spin Peltier effect for magnetic insulators," *Phys. Rev. Lett.*, vol. 113, 027601, doi: 10.1103/PhysRevLett.113.027601.

Fu H-R, Chang C-R, Wang Y-K, Evans R F L, Chantrell R W, Jeng H-T (2016), "Newtype single-layer magnetic semiconductor in transition-metal dichalcogenides VX_2 (X = S, Se and Te)," *Sci. Rep.*, vol. 6, 32625; doi: 10.1038/srep32625.

Gao D, Xue Q, Mao X, Wang W, Xu Q, Xue D (2013), "Ferromagnetism in ultrathin VS_2 nanosheets," *J. Mater. Chem. C*, vol. 1, pp. 5909–5916, doi: 10.1039/C3TC31233J.

Hahn C, de Loubens G, Klein O, Viret M, Naletov V V, Ben Youssef J (2013), "Comparative measurements of inverse spin Hall effects and magnetoresistance in YIG/Pt and YIG/Ta," *Phys. Rev. B*, vol. 87, 174417, doi: 10.1103/PhysRevB.87.174417.

Hansen P, Witter K, Tolksdorf W (1983), "Magnetic and magneto-optic properties of lead- and bismuth-substituted yttrium iron garnet films," *Phys. Rev. B*, vol. 27, pp. 6608–6625, doi: 10.1103/PhysRevB.27.6608.

Heinrich B, Burrowes C, Montoya E, Kardasz B, Girt E, Song Y-Y, Sun Y, Wu M (2011), "Spin pumping at the magnetic insulator (YIG)/normal metal (Au) interfaces," *Phys. Rev. Lett.*, vol. 107, 066604, doi: 10.1103/PhysRevLett.107.066604.

Heyd J, Scuseria G E, Ernzerhof M (2003), "Hybrid functionals based on a screened Coulomb potential," *J. Chem. Phys.*, vol. 118, pp. 8207–8215, doi: 10.1063/1.1564060.

Heyd J, Scuseria G E, Ernzerhof M (2006), "Erratum: Hybrid functionals based on a screened Coulomb potential," *J. Chem. Phys.*, vol. 124, 219906, doi: 10.1063/1.2204597.

Hoffmann A (2013), "Spin Hall effects in metals," *IEEE Trans. Magn.*, vol. 49, pp. 5172–5193, doi: 10.1109/TMAG.2013.2262947.

Zhuang H L, Hennig R G (2016), "Stability and magnetism of strongly correlated single-layer VS_2," *Phys. Rev. B*, vol. 93, 054429, doi: 10.1103/PhysRevB.93.054429.

Hahn C, de Loubens G, Klein O, Viret M, Naletov V V, Ben Youssef J (2013), "Comparative measurements of inverse spin Hall effects and magnetoresistance in YIG/Pt and YIG/Ta," *Phys. Rev. B.*, vol. 87, 174417, doi: 10.1103/PhysRevB.87.174417.

Jaworski C M, Yang J, Mack S, Awschalom D D, Heremans J P, Myers R C (2010), "Observation of the spin-Seebeck effect in a ferromagnetic semiconductor," *Nature Mater.*, vol. 9, pp. 898–903, doi: 10.1038/nmat2860.

Kimura T, Kawamoto S, Yamada I, Azuma M, Takano M, Tokura Y (2003), "Magnetocapacitance effect in multiferroic $BiMnO_3$," *Phys. Rev. B*, vol. 67, 180401, doi: 10.1103/PhysRevB.67.180401.

Kresse G, Hafner J (1993), "*Ab initio* molecular dynamics for open-shell transition metals," *Phys. Rev. B*, vol. 48, pp. 13115–13118, doi: 10.1103/PhysRevB.48.13115.

Kresse G, Joubert D (1999), "From ultrasoft pseudopotentials to the projector augmented-wave method," *Phys. Rev. B*, vol. 59, pp. 1758–1775, doi: 10.1103/PhysRevB.59.1758.

Kuc A, Zibouche N, Heine T (2011), "Influence of quantum confinement on the electronic structure of the transition metal sulfide TS_2," *Phys. Rev. B*, vol. 83, 245213, doi: 10.1103/PhysRevB.83.245213.

Kumar A, He H, Pandey R, Ahluwalia P K, Tankeshwar K (2015), "Pressure and electric field-induced metallization in the phase-engineered ZrX_2 (X = S, Se, Te) bilayers," *Phys. Chem. Chem. Phys.*, vol. 17, pp. 19215–19221, doi: 10.1039/C5CP01445J.

LeClair P, Ha J K, Swagten H J M, Kohlhepp J T (2002), "Large magnetoresistance using hybrid spin filter devices," *Appl. Phys. Lett.*, vol. 80, pp. 625–627, doi: 10.1063/1.1436284.

Liechtenstein A I, Anisimov V I, Zaane J (1995), "Density-functional theory and strong interactions: Orbital ordering in Mott-Hubbard insulators," *Phys. Rev. B*, vol. 52, pp. R5467–R5470, doi: 10.1103/PhysRevB.52.R5467.

Ma Y D, Dai Y, Wei W, Niu C, Yu L, Huang B (2011), "First-principles study of the Graphene@$MoSe_2$ heterobilayers," *J. Phys. Chem. C*, vol. 115, pp. 20237–20241, doi: 10.1021/jp205799y.

Ma Y, Dai Y, Guo M, Niu C, Zhu Y, Huang B (2012), "Evidence of the existence of magnetism in pristine VX_2 monolayers (X = S, Se) and their strain-induced tunable magnetic properties," *ACS Nano*, vol. 6, pp. 1695–1701, doi: 10.1021/nn204667z.

Marseglia E A (1983), "Transition metal dichalcogenides and their intercalates," *Int. Rev. Phys. Chem.*, vol. 3, pp. 177–216, doi: 10.1080/01442358309353343.

Matthias B T, Bozorth R M, Van Vleck J H (1961), "Ferromagentic interaction in EuO," *Phys. Rev. Lett.*, vol. 7, pp. 160–161, doi: 10.1103/PhysRevLett.7.160.

Meziane S, Feraoun H, Ouahrani T, Esling C (2013), "Effects of Li and Na intercalation on electronic, bonding and thermoelectric transport properties of MX_2 (M = Ta; X = S or Se) dichalcogenides—Ab initio investigation," *J. Alloy Compd.*, vol. 581, pp. 731–740, doi: 10.1016/j.jallcom.2013.07.033.

Miao B F, Huang S Y, Qu D, Chien C L (2014), "Physical origins of the new magnetoresistance in Pt/YIG," *Phys. Rev. Lett.*, vol. 112, 236601, doi: 10.1103/PhysRevLett.112.236601.

Montoya E, Heinrich B, Girt E (2014), "Quantum well state induced oscillation of pure spin currents in Fe/Au/Pd(001) systems," *Phys. Rev. Lett.*, vol. 113, 136601, doi: 10.1103/PhysRevLett.113.136601.

Moodera J S, Hao X, Gibson G A, Meservey R (1988), "Electron-spin polarization in tunnel junctions in zero applied field with ferromagnetic EuS barriers," *Phys. Rev. Lett.*, vol. 61, pp. 637–620, doi: 10.1103/PhysRevLett.61.637.

Perdew J P, Burke K, Ernzerhof M (1996), "Generalized gradient approximation made simple," *Phys. Rev. Lett.*, vol. 77, pp. 3865–3868, doi: 10.1103/PhysRevLett.77.3865.

Radisavljevic B, Radenovic A, Brivio J, Giacometti V, Kis A (2011), "Single-layer MoS_2 transistors," *Nature Nanotechnol.*, vol. 6, pp. 147–150, doi: 10.1038/nnano.2010.279.

Rogado N S, Li J, Sleight A W, Subramanian M A (2005), "Magnetocapacitance and magnetoresistance near room temperature in a ferromagnetic semiconductor: La_2NiMnO_6," *Adv. Mater.*, vol. 17, pp. 2225–2227, doi: 10.1002/adma.200500737.

Solovyev I V, Dederichs P H, Anisimov V I (1993), "Corrected atomic limit in the local-density approximation and the electronic structure of *d* impurities in Rb," *Phys. Rev. B*, vol. 50, pp. 16861–16871, doi: 10.1103/PhysRevB.50.16861.

Splendiani A, Sun L, Zhang Y, Li T, Kim J, Chim C-Y, Galli G, Wang F (2010), "Emerging photoluminescence in monolayer MoS_2," *Nano Lett.*, vol. 10, pp. 1271–1275, doi: 10.1021/nl903868w.

Uchida K A, Ota T, Nakayama H, Maekawa S, Saitoh E (2010), "Observation of longitudinal spin-Seebeck effect in magnetic insulators," *Appl. Phys. Lett.*, vol. 97, 172505, doi: 10.1063/1.3507386.

Wang Q H, Kalantar-Zadeh K, Kis A, Coleman J N, Strano M S (2012), "Electronics and optoelectronics of two-dimensional transition metal dichalcogenides," *Nature Nanotechnol.*, vol. 7, pp. 699–712, doi: 10.1038/nnano.2012.193.

Wolf S A, Awschalom D D, Buhrman R A, Daughton J M, von Molnár S, Roukes M L, Chtchelkanova A Y, Treger D M (2001), "Spintronics: A spin-based electronics vision for the future," *Science*, vol. 294, pp. 1488–1495, doi: 10.1126/science.1065389.

Xiao D, Liu G-B, Feng W, Xu X, Yao W (2012), "Coupled spin and valley physics in monolayers of MoS_2 and other group-VI dichalcogenides," *Phys. Rev. Lett.*, vol. 108, 196802, doi: 10.1103/PhysRevLett.108.196802.

Zhang H, Liu L M, Lau W M (2013), "Dimension-dependent phase transition and magnetic properties of VS_2," *J. Mater. Chem. A*, vol. 1, pp. 10821–10828, doi: 10.1039/C3TA12098H.

Zhao K, Deng Z, Wang X C, Han W, Zhu J L, Li X, Liu Q Q, Yu R C, Goko T, Frandsen B, Liu L, Ning F, Uemura Y J, Dabkowska H, Luke G M, Luetkens H, Morenzoni E, Dunsiger S R, Senyshyn A, Böni P, Jin C Q (2013), "New diluted ferromagnetic semiconductor with Curie temperature up to 180 K and isostructural to the '122' iron-based superconductors," *Nature Commun.*, vol. 4, 1442, doi: 10.1038/ncomms2447.

Zhu Z Y, Cheng Y C, Schwingenschlögl U (2011), "Giant spin-orbit-induced spin splitting in two-dimensional transition-metal dichalcogenide semiconductors," *Phys. Rev. B*, vol. 84, 153402, doi: 10.1103/PhysRevB.84.153402.